frontiers | Frontiers in Marine Science

ORIGINAL RESEARCH
published: 15 July 2022
doi: 10.3389/fmars.2022.891876

Field Application of Automated Spectrophotometric Analyzer for High-Resolution *In Situ* Monitoring of pH in Dynamic Estuarine and Coastal Waters

Münevver Nehir[1*], *Mario Esposito*[1], *Socratis Loucaides*[2] *and Eric P. Achterberg*[1]

[1] *Marine Biogeochemistry, Chemical Oceanography GEOMAR Helmholtz Centre for Ocean Research Kiel, Kiel, Germany*,
[2] *Ocean Technology and Engineering, National Oceanography Centre, Southampton, United Kingdom*

OPEN ACCESS

Edited by:
Laura Lorenzoni,
National Aeronautics and Space Administration (NASA), United States

Reviewed by:
Mike D. DeGrandpre,
University of Montana, United States
Ellen Briggs,
University of Hawaii at Manoa, United States
Xuewu Liu,
University of South Florida, United States

***Correspondence:**
Münevver Nehir
mnehir@web.de

Specialty section:
This article was submitted to Marine Biogeochemistry, a section of the journal Frontiers in Marine Science

Received: *08 March 2022*
Accepted: *08 June 2022*
Published: *15 July 2022*

Citation:
Nehir M, Esposito M, Loucaides S and Achterberg EP (2022) Field Application of Automated Spectrophotometric Analyzer for High-Resolution In Situ Monitoring of pH in Dynamic Estuarine and Coastal Waters. Front. Mar. Sci. 9:891876. doi: 10.3389/fmars.2022.891876

High quality pH measurements are required in estuarine and coastal waters to assess the impacts of anthropogenic atmospheric CO_2 emissions on the marine carbonate system, including the resulting decrease in pH. In addition, pH measurements are needed to determine impacts on carbonate chemistry of phytoplankton blooms and their breakdown, following enhanced anthropogenic nutrient inputs. The spectrophotometric pH technique provides high quality pH data in seawater, and is advantageous for long-term deployments as it is not prone to drift and does not require *in situ* calibration. In this study, a field application of a fully automated submersible spectrophotometric analyzer for high-resolution *in situ* pH measurements in dynamic estuarine and coastal waters is presented. A Lab-on-Chip (LOC) pH sensor was deployed from a pontoon in the inner Kiel Fjord, southwestern Baltic Sea, for a total period of 6 weeks. We present a time-series of *in situ* pH_T (total pH scale) and ancillary data, with sensor validation using discretely collected samples for pH_T and laboratory analysis. The difference between the sensor and laboratory analyses of discrete samples was within ±0.015 pH_T unit, with a mean difference of 0.001 (n=65), demonstrating that the LOC sensor can provide stable and accurate pH_T measurements over several weeks.

Keywords: pH sensor, Lab-on-Chip, spectrophotometric, mCP, Kiel Fjord, coastal carbonate system, ocean acidification

INTRODUCTION

The oceans play a significant role in the global carbon cycle as one of the main reservoirs of carbon. Since the beginning of the Industrial Revolution, anthropogenic CO_2 emissions have perturbed the exchange of CO_2 between the atmosphere and oceans. Oceans have absorbed about a quarter of anthropogenic carbon dioxide (CO_2) emissions (Friedlingstein et al., 2020), a process causing a long-term pH decrease (ocean acidification). To date, several studies have focused on determining the progression of ocean acidification by using long-term ocean observations datasets (Dore et al., 2009; Midorikawa et al., 2010; Hu et al., 2015; Van Dam and Wang, 2019; Ishida et al., 2021). Time-series measurements of surface ocean pH over the past two decades have reported a decrease of about 0.1 units since the pre-industrial era from ca. 8.2 to 8.1 (Orr et al., 2005). An additional

decrease in surface ocean pH of more than 0.4 units is expected by the end of the 21st century (Feely et al., 2009; Jiang et al., 2019; Kwiatkowski et al., 2020).

Estuarine and coastal waters are more complex than open ocean waters and are highly dynamic environments where freshwater discharges mix with seawater, with many systems impacted by anthropogenic activities. For example, nutrient run-off results in eutrophication with the ensuing breakdown of organic matter produced by phytoplankton blooms causing high pCO_2 and reduced pH values, adding to the acidification caused by anthropogenic CO_2 uptake (Wallace et al., 2014; Zhao et al., 2020). The acidification of estuarine and coastal waters is affecting ecosystems negatively and various biogeochemical processes in a water column (Guinotte and Fabry, 2008; Hall et al., 2020; Thomas et al., 2022). For example, enhanced acidic conditions threaten the growth, abundance, and survival of shell-forming organisms (corals, some plankton species, and commercial shellfish (Doney et al., 2020; Fox et al., 2020; Wilson et al., 2020; Blaisdell et al., 2021) and affect the solubility and speciation of trace metals (Millero et al., 2009; Hoffmann et al., 2012). To improve our understanding of the current state of the kinetics and dynamics of various physical and biogeochemical processes in estuarine and coastal waters, monitoring activities with a high-resolution are essential (Carstensen et al., 2018), and pH is one of the keystone parameters to be observed.

High-resolution measurements of pH are essential for tracking the thermodynamic state of acid-base processes in seawater. pH is a measure of the concentrations of hydrogen ion on a logarithmic scale and one of the four measurable parameters of the marine carbonate system. Others are the partial pressure of carbon dioxide (pCO_2), dissolved inorganic carbon (DIC) and total alkalinity (A_T) (Millero, 2007). The gaseous form of CO_2 dissolve in surface waters and is converted into carbonic acid (H_2CO_3), hydrogen (H^+), bicarbonate (HCO_3^-), carbonate (CO_3^{2-}) ions (Dickson et al., 2007) as follows:

$$CO_{2(g)} \leftrightarrow CO_{2(aq)}$$

$$CO_{2(aq)} + H_2O_{(l)} \leftrightarrow H_2CO_3(aq)$$

$$H_2CO_3(aq) \leftrightarrow HCO_3^-(aq) + H^+(aq)$$

$$HCO_3^-(aq) \leftrightarrow CO_3^{2-}(aq) + H^+(aq)$$

Four different seawater pH scales; NBS (U.S. National Bureau of Standards), free, total, and seawater, are described in literature and the total scale is favored in oceanography as it includes the effect of sulfate ions (Mosley et al., 2004; Riebesell et al., 2010; Fassbender et al., 2021). The calculation of the dissociation constant of the sulfate ion can be eliminated using the total proton scale (Zeebe and Wolf-Gladrow, 2001). All pH data reported in this study are on the total $[H^+]_T$ scale, expressed as:

$$pH_T = H^+ + HSO_4^-.$$

The traditional carbonate chemistry observations in marine systems are based on discrete water sample collection, storage, transportation, and land-based laboratory analysis. Discrete water samples for carbonate chemistry can be collected using dedicated samplers such as Niskin bottles, and then stored following poisoning using mercuric chloride until laboratory analysis for pH, DIC and A_T using standard operational procedures (Dickson et al., 2007). pH can be determined directly using potentiometric or spectrophotometric techniques (Dickson et al. (2007), but also calculated *via* the CO2Sys software following e.g. A_T and DIC measurements (Lewis and Wallace, 1998; Pierrot et al., 2006). The main limitations of this approach are the inadequate temporal resolution and duration and the high costs associated with the collection, preservation, shipping, and analysis of samples.

Advancements in marine technology and observational oceanography have enabled the development of miniaturized *in situ* pH sensors that can be integrated into stationary or autonomous platform for monitoring marine environments at a high temporal and spatial resolution (Sastri et al., 2019). To date, a range of pH sensors have been reported for autonomous *in situ* pH measurements, and are based on three different analytical methods, potentiometry (electrodes), fluorescence (optodes) and, spectrophotometry (indicator dyes). **Table 1** presents examples of the current *in situ* pH sensors and their application in multiple oceanographic studies. Each system has a range of advantages and limitations (Rérolle et al., 2012; Rérolle et al., 2018; Sastri et al., 2019). Potentiometric pH sensors for seawater (i.e., Honeywell Durafet Ion-Sensitive Field Effect Transistor (ISFET), SeaFET, SeapHOx) do not require chemical reagents and have a fast sampling frequency (6 seconds per measurement), but measurements are limited to a salinity range between 20 and 40 (Sea-Bird Electronics, Inc.). Besides, Honeywell Durafet based pH sensors may be prone to drift (potentially more than 0.02 pH unit/week) (Rérolle et al., 2016), therefore require preconditioning of the electrode for 5 to 10 days and frequent calibrations (Sabine et al., 2004; Martz et al., 2010; Bresnahan et al., 2014; Mclaughlin et al., 2017; Miller et al., 2018). To date, the Deep Sea Durafet sensor has been deployed on a range of profiling floats, and the assessment and correction for any potential drift to reduce bias in the pH measurements have been comprehensively evaluated by Johnson et al., 2016. Recent work introduced a self-calibrating SeapHOx system for seawater, periodic flushing of the sample cell with a calibration solution of Tris buffer in artificial seawater (Bresnahan et al., 2021), which is yet limited to seawater applications. The main limitations of fluorescent-based pH measurements are the interfering compounds of natural seawater (i.e., chlorophyll-a), drift with time, and the sensor spot is also light sensitive (Clarke et al., 2015). Staudinger et al. (2018) presented a stand-alone optode sensor system for pH, oxygen, and carbon dioxide with an integrated battery and logger and its short-term applications in the Baltic Sea and mentioned the need for drift correction and assessment of biofouling for long-term deployments.

The spectrophotometric method for pH, developed in the 1980s (Robert-Baldo et al., 1985), provides many advantages for marine studies as it is robust, stable, calibration-free

TABLE 1 | Examples of the current in situ pH sensors used in oceanographic studies.

Model, Manufacturer	Analytical method	pH Monitoring Applications
Honeywell Durafet ISFET, SeaFET and SeapHOx (Sea-Bird Electronics, USA)	Potentiometric	Deployment of ISFET pH sensor on vertical profiling platforms from 2000 m to the surface over several months (Johnson et al., 2016):<0.010 pH units accuracy. Deployment of ISFET pH sensor in coastal waters over months periods (Bresnahan et al., 2014):<0.030 pH units accuracy. Commercially available SeaFET and SeapHOx sensors based on ISFET technology: ± 0.050 pH units accuracy (https://www.seabird.com/seafet-v2-ocean-ph-sensor/product-details?id=54627921732&callback=qs). SeaFET pH sensor deployment in coastal waters of south-central Alaska, USA for a period of 3 to 5 months (Miller et al., 2018):<0.025 pH units accuracy.
pH optodes (Custom-made)	Fluorescent optode	Shipboard surface seawater measurements in the Southern Ocean, over a month (Clarke et al., 2015): accuracy is not reported, 0.0074 pH units precision. Profiling on a pier in Southampton, UK, for 6 days (Staudinger et al., 2018): 0.020 pH units accuracy.
SAMI-pH (Sunburst Sensors, LLC, USA)	Spectrophotometric	Coastal waters, deployment at the pier at Scripps Institution of Oceanography for about 22 days (Seidel et al., 2008): ± 0.0017 pH units accuracy. Commercially available SAMI-pH sensor: ± 0.003 pH units accuracy (http://www.sunburstsensors.com/products/oceanographic-ph-sensor.html).
CONTROS HydroFIA-pH (4H-Jena engineering GmbH, Germany)	Spectrophotometric	Shipboard measurements in the North Sea over 6 weeks period (Aßmann et al., 2011): 0.0081 pH units accuracy compared to CRM and 0.0005 pH units to a reference system, short-term precision: ± 0.0007. Note: The sensor is a benchtop unit, not yet submersible.
National Oceanography Centre, University of Southampton, UK, Lab-on-Chip pH (ClearWater Sensors, Southampton, UK)	Spectrophotometric	Deployed in surface waters of northwest European shelf seas for about a month period (Rérolle et al., 2018): 0.004 pH units accuracy compared to CRM. Deployed on fixed and moving platforms over varying environmental salinity, temperature, and pressure condition (Yin et al., 2021): +0.003 ± 0.022 pH units accuracy compared to discrete validation seawater samples.

and not prone to drift (Rérolle et al., 2012). Under oceanic conditions, spectrophotometric pH measurement systems have demonstrated excellent performance (Clayton and Byrne, 1993; Bellerby et al., 2002; Aßmann et al., 2011; Rérolle et al., 2016). Commercially available, submersible spectrophotometric sensors (see **Table 1**, Lab-on-Chip (LOC) and SAMI-pH) have been successfully tested for fine-scale, autonomous and *in situ* monitoring of pH in a wide variety of environments, from freshwater (Martz et al., 2003) to seawater (Seidel et al., 2008; Rérolle et al., 2018; Yin et al., 2021). Indicator impurities and wavelength accuracy of spectrophotometers are some of the potential sources of uncertainty in spectrophotometric pH measurements, which DeGrandpre et al. (2014) has reported in detail. The quality of the pH data is related to how well the molar extinction coefficients and the second dissociation constant of an indicator dye have been determined as a function of sample temperature and salinity. To date, the experimental characterization and modelling of a meta-Cresol Purple (mCP) for estuarine ($S \leq 20$, Mosley et al., 2004; Lai et al., 2016; Douglas and Byrne, 2017; Lai et al., 2017; Müller and Rehder, 2018) and hypersaline ($35 \leq S \leq 100$, Loucaides et al., 2017) waters have been reported.

Recently, the capabilities of the LOC pH sensor have been successfully demonstrated on fixed and moving platforms under different environmental conditions, including deployments in surface waters of Southampton ($S>24$) for several months, and in deep ocean waters (~4820 m) (Yin et al., 2021). However, the performance of this LOC pH sensor in estuarine and coastal waters has not yet been thoroughly investigated.

The aim of this study was to evaluate the performance of an automated spectrophotometric analyzer, a LOC sensor, for high-resolution *in situ* pH determinations in dynamic estuarine and coastal waters, and expand the applicability of the sensor to waters with a wide salinity range (13.2-21.8). The sensor was deployed from a floating pontoon at GEOMAR Helmholtz Centre for Ocean Research (Kiel, Germany) in the southwestern Baltic Sea between summer and autumn 2018 for a total period of 6 weeks. Ancillary data were obtained to assess the control of pH dynamics at the sampling site. Additional spectrophotometric pH_T measurements were conducted in the laboratory on discretely collected samples, and the measurements were validated with certified reference material (DIC-A_T CRM, Batch-151, obtained from Prof. A. G. Dickson at Scripps Institute of Oceanography, USA).

MATERIALS AND METHODS

Sensor Overview

The LOC pH sensor is a submersible unit that performs autonomous *in situ* pH analysis with a spectrophotometric technique using microfluidic components and was initially developed in 2012 by the Ocean Technology and Engineering group at National Oceanography Centre (NOC) and University of Southampton, UK (Rérolle et al., 2013). It is now (since 2021) commercially available from ClearWater Sensors, Southampton, UK. A schematic diagram of the fluidic design of the sensor is shown in **Figure 1**. All components were mounted on a three-layer microfluidic chip made from tinted poly(methylmethacrylate) (PMMA, (Floquet et al., 2011; Perez et al., 2016), and together with the electronics placed in a mineral oil-filled (M3516 from Merck, viscosity ≤ 30.0cps) pressure compensated, watertight cylindrical polyvinylchloride housing (15 cm diameter, 56 cm height, 920 g weight in air). Detailed information of the sensor housing and microfluidic chip unit can be found in (Grand et al., 2017).

The operation of the sensor is explained in brief here. A sample and indicator dye are injected by two separate syringe pumps, controlled by valves, and mixed in a static mixer before entering a 10 mm optical cell. The change in the intensity of light transmitted by a Light Emitting Diode (LED, Roithner Lasertechnik, Austria) at 435 nm (15 nm full width at half maximum (FWHM)) and 590 nm (15 nm FWHM) through the optical cell is recorded by a photodiode detector (TSL257, TAOS Inc., USA) (Floquet et al., 2011; Rérolle et al., 2013; Perez et al., 2016). To account for slight discrepancies between the wavelengths of the LED's emission and the mCP's absorption maxima (434 and 578 nm) the pH sensor is calibrated post-manufacture according to Yang et al. (2014). The ratio of absorbances at the absorbance maxima of the acidic and basic forms of the indicator dye is then used to assess the pH value of a sample (Clayton and Byrne, 1993). In continuous operation mode, the sensor requires low power about 3 W or 1300 J per measurement and one measurement takes approximately 8 minutes (Yin et al., 2021). For each measurement, 3 µl of indicator dye is added to 700 µl of sample according to a pre-programmed measurement routine stored internally on the sensor unit. Approximately 0.4 mL of indicator is consumed per day when the sensor operates in continuous mode. Stock solutions of mCP are stored in 50 mL gas impermeable Flexboy bags (Sartorius Stedim Biotech, UK), wrapped in black tape to protect from light and avoid photo bleaching. The mCP stock solution remains stable for several months up to 2 years, when stored appropriately (Takeshita et al., 2021). It is possible to conduct up to 16.666 analyses with one reagent bag of 50 mL, which was attached externally to the LOC pH unit. Waste was collected into an additional external bag attached to the sensor. The WetChem Graphical User Interface (GUI) was used to operate the sensor and visualize intensity values, measurement time, pump position, internal temperature in real-time.

Analytical Principle and Data Processing of the LOC pH Sensor

The analytical principle of spectrophotometric pH determination is based on an addition of a pH-sensitive diprotic sulfonephthalein indicator dye (H_2I) to a water sample. The dye changes color according to the pH of the seawater sample, i.e., the color changes from pink to yellow when it is in the acidic [HI^-] and to purple when it is in the more basic [I^{2-}] form (Clayton and Byrne, 1993). Chemical equilibria between three dissociation forms of the dye can be expressed as follows:

$$H_2I \overset{K_1}{\Leftrightarrow} HI^- + H^+ \qquad K_1 = \frac{\left[H_2I\right]}{\left[H^+\right]\bullet\left[HI^-\right]} \quad (1)$$

$$HI^- \overset{K_2}{\Leftrightarrow} I^{2-} + H^+ \qquad K_2 = \frac{\left[HI^-\right]}{\left[H^+\right]\bullet\left[I^{2-}\right]} \quad (2)$$

where [] indicates concentration, K_1 and K_2 are first and second dissociation constant of the indicator, respectively. The pK_2 (in other terms $-log(K_2)$) of mCP is close to the pH of seawater, which is typically between 7.6 to 8.3 (Dickson et al., 2007).

The pH of a seawater sample (pH=$-log[H^+]$) can then be quantified as:

$$pH_T = -log\left(K_2\right) + \log\left(\frac{\left[I^{2-}\right]}{\left[HI^-\right]}\right) \quad (3)$$

According to the *Beer-Lambert Law*, the amount of [I^{2-}] and [HI^-] can be calculated using their distinct absorption properties at 434 and 578 nm:

$$A_\lambda = \left(\epsilon_\lambda^{I^{2-}} \bullet \left[I^{2-}\right] + \epsilon_\lambda^{HI^-} \bullet \left[HI^-\right]\right) \bullet l \quad (4)$$

where A_λ is the absorbance, ε_λ is the molar absorptivity values at wavelength λ, and l is the optical path length.

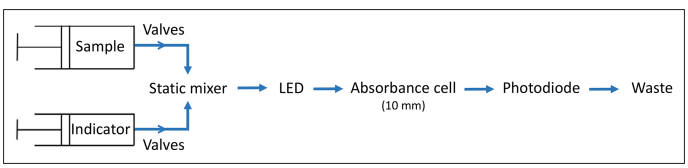

FIGURE 1 | The schematic diagram of the fluidic design of the LOC pH sensor.

Then, the equation used to quantify pH can be rearranged as follows:

$$pH_T = -\log(K_2 e_2) + \log\left(\frac{R - e_1}{1 - R\bullet\frac{e_3}{e_2}}\right) \quad (5)$$

$$\text{where } e_1 = \frac{\epsilon_{578}^{[HI^-]}}{\epsilon_{434}^{[HI^-]}},\ e_2 = \frac{\epsilon_{578}^{[I^{2-}]}}{\epsilon_{434}^{[HI^-]}},\ e_3 = \frac{\epsilon_{434}^{[I^{2-}]}}{\epsilon_{434}^{[HI^-]}}$$

where R is the ratio of absorbance at 578 (maximum peak for $[I^{2-}]$) to 434 nm (maximum peak for $[HI^-]$), R = A_{578}/A_{434} (Clayton and Byrne, 1993; Liu et al., 2011).

A recent study reports on the characterization of a range of sulfonephthalein indicator dyes in detail, including mCP, for a broad range of environmental conditions (Hudson-Heck et al., 2021). Data processing of the LOC sensors raw data involves computation of molar extinction coefficients (in terms of *e1, e3/e2*), and second dissociation constant value (pK_2) of mCP at sample temperature and salinity using the equations and coefficients obtained from the literature (*e1, e3/e2* were computed from (Liu et al., 2011) and $pK_2$was computed from Müller and Rehder, 2018, which is valid for salinity range 5-20 and temperature range 5-35°C). *In situ* temperature and salinity data of the sample were collected in parallel by external sensors (see section 2.3.).

In this study, a purified mCP (Acros Organics, 99%) indicator dye was used as its ε_λ and $pK_2$are well-established for estuarine waters (Lai et al., 2016; Lai et al., 2017; Müller and Rehder, 2018). The purification of mCP was done by following the protocol described in Liu et al. (2011) and Loucaides et al. (2017). A 4 mM mCP reagent solution adjusted to pH 8.0 ± 0.1 at 25°C was prepared and verified by a glass pH electrode.

Field Deployments: Sampling Site and Ancillary Data

In situ field demonstration of the LOC pH sensor was performed on a floating pontoon facility of GEOMAR (Kiel, Germany; 54°19'48.78"N, 10° 8'59.44"E) for a period of 6 weeks between August 1st to 13th and October 20th to November 19th, 2018. The sampling site is surrounded by dockyards and cruise ship terminals, and the city of Kiel with a population of ca. 250,000. The Kiel Fjord has a length of 9.5 km, an inner width of 250 m with depth of 10 to 12 m, an outer width of up to 7.5 km with depths greater than 20 m (Nikulina et al., 2008). The fjord drains into the southwest Baltic Sea. The waters in the inner fjord are homogeneously mixed, except during the summer period following water column stratification. Most of the freshwater delivered to the system is from rainwater and the Schwentine River on the eastern shore (Nikulina et al., 2008).

The LOC sensor was programmed to sample at hourly intervals (except for the first 5 days in August: 20 min intervals). A 0.45 µm Millex HP PES in-line filter (Millipore, Merck, Darmstadt, Germany) was placed at the sample inlet of the LOC sensor to prevent particles from entering the microfluidic channels (Rérolle et al., 2013). The filter surface area is relatively large compared to the volume of sample withdrawn and therefore no significant underpressure is required to draw sample through. The sensor was powered externally by a 12 V power supply.

Salinity, temperature and oxygen were measured with a sampling interval of one minute using a SBE 37-SMP-ODO MicroCAT CTD and dissolved oxygen (DO, dO_2) sensor (Sea-Bird Electronics, USA). The LOC, CTD, and DO sensors were mounted on a stainless steel sensor frame that was lowered from the side of the pontoon and positioned at a depth of ca 2 m. Discrete water samples were collected daily, once in the morning and/or once in the evening, using a peristaltic pump (Cole Palmer, Masterflex L/S series) placed on the floating pontoon. The inlet of an acid cleaned (with 1 M HCl) 6.4 mm ID C-Flex tubing (Cole Palmer Masterflex) was attached to the frame close to the sample inlet of the LOC pH sensor. Discrete seawater samples for direct spectrophotometric laboratory analysis of pH_T (Yin et al., 2021) were pumped into 250 mL borosilicate bottles and sealed with a ground stopper. Analyses of unpreserved samples were performed within few hours in the laboratory using a benchtop spectrophotometric CONTROS HydroFIA pH analyzer (4H-Jena engineering GmbH, Aßmann et al., 2011). Measurements of the LOC sensor and HydroFIA analyzer were validated using the DIC-A_T CRM (Batch-151, pH_T 7.862 at temperature 25°C and salinity 33) from Prof. A. G. Dickson (Scripps Institute of Oceanography, USA) before and after deployments. The correction of sample pH_T was done using equations described in section 2.2 and *in situ* temperature and salinity values. Seawater samples of inorganic nutrients (NO_3^-, PO_4^{3-} and SiO_4^{-4}) were collected after filtration through an AcroPak 500 (Pall GmbH, Germany) in acid-cleaned (1 M HCl) 50 mL polypropylene centrifuge tubes (Jet Bio-Filtration Co., Ltd., Guangzhou, China) and stored at -20°C for about a month until the wet-chemical colorimetric laboratory analysis using a Seal QuAAtro autoanalyser (Becker et al., 2019).

The GEOMAR pontoon facility is used for continuous time-series measurements of various biogeochemical and physical parameters in Kiel Fjord as part of the KIMOCC environmental data monitoring program. Here, we used the one-minute interval post-processed pCO_2 data of the installed CONTROS HydroC CO_2 sensor (4H-Jena engineering GmbH, Germany). An overview of the analytical principle of the CO_2 sensor and data processing can be found in Fietzek et al. (2014). CO2Sys was used to calculate concentration of dissolved CO_2 gas in the water sample. Throughout the study, *in situ* pCO_2 levels are in µatm and dissolved CO_2 gas levels are in µmol·kg^{-1} SW.

Weather data (wind speed, rainfall, solar irradiation) were obtained from the GEOMAR weather station, and were available for every 8 min. The tide gauge water level (meter) measurements at Kiel Fjord were obtained from the IOC Sea Level Monitoring Facility (http://www.ioc-sealevelmonitoring.org/station.php?code=kiel). All sensors and ancillary data presented throughout this study were examined and processed using Python software (version 3.7.4).

RESULTS AND DISCUSSION

Validation of *In Situ* pH Sensor Measurements

A total of 65 individual samples were collected during deployments that were analyzed employing a benchtop spectrophotometric analyzer to ensure the accuracy of pH values reported using the LOC sensor. The LOC sensor and discrete water samples pH data followed a consistent pattern throughout both deployments (**Figure 2A**) and were significantly indifferent (a paired t-test, $p \leq 0.05$). A linear regression yielded y=0.998x+0.004 ($R^2 = 0.99$) for a total of 65 samples. No offset was applied to the sensor data and both sensor and discrete pH results were calculated independently. The average difference between the sensor and discrete samples pH (ΔpH_T=LOC sensor-discrete water samples) was 0.001 pH units, but ranged from -0.015 to 0.015 over the duration of the summer and autumn deployments (**Figure 3**). No clear correlation was found between ΔpH_T and ancillary data (T, S, dO_2), however, the relationship between pH_T and ancillary data will be detailed in the next section. Additional validation of the sensor pH measurements was done by calculating pH_T from salinity-derived A_T and *in situ* pCO_2. Computational details of salinity-derived A_T will be clarified in section 3.2. pH data from the summer and autumn deployments pooled together and for a total pH value of 978, a linear regression analysis resulted in $R^2 = 0.86$, with an equation of y=1.030x-0.217 (**Figure 2B**).

Both the LOC sensor and HydroFIA analyzer measurements were validated by consecutive measurements of DIC-TA Certified Reference Material (CRM) (Batch-151, pH_T=7.862 at T=25°C, S=33) before and after the field deployments. The mean pH values obtained from ten consecutive CRM measurements in July, September, and November 2018 were 7.858 ± 0.002, 7.860 ± 0.002 and 7.859 ± 0.001 pH units for the LOC pH sensor and 7.861 ± 0.001, 7.862 ± 0.002 and 7.860 ± 0.001 pH units for the HydroFIA pH analyzer. Both analyzers had a precision of about 0.001 pH units, and the accuracy of the measurements were slightly better with the HydroFIA analyzer (<0.002 pH units).

Statistical Distribution and Diel Variations of *In Situ* pH and Ancillary Data

The main focus of this work was to demonstrate the capability of the LOC pH sensor in a highly dynamic system, and analysis of the biogeochemical data was completed to investigate the biogeochemical processes influencing carbonate chemistry dynamics in the Kiel Fjord. The statistical distribution of all data (seawater temperature, salinity, pH_T, dO_2, pCO_2, NO_3^-, PO_4^{3-} and SiO_4^{-4} is presented in **Table 2** and allows a closer examination of the summer and autumn data. The seawater temperature and salinity, characterizing the hydrographic situation, showed marked changes; the mean salinity values were about 4 units higher and the mean temperature values were about 10 units lower in autumn, indicating saltier and colder water intrusion in the fjord, with fresher waters in summer. Highly dynamic salinity conditions for Kiel Fjord ranging from 2.6 to 22.4 have been reported, with a mean of 14.3 (Schories et al., 2006). During our summer deployment the salinity values ranged between 13.2 and 18 (mean 15.7), and in autumn deployment within 19.6 to 21.8 (mean 20.7). Enhanced seawater temperatures ranging between 18.1 and 24.2°C (mean 22.1°C) characterized the summer deployment. In autumn, temperature dropped to a minimum value of 8.7 and ranged up to 14.1°C (mean 11.5°C).

The LOC sensor determined *in situ* pH_T values were within 7.520-8.275 (mean 7.954) and within 7.560-7.932 (mean, 7.742) in summer and autumn, respectively. High mean pCO_2 levels were observed related to lower pH values towards autumn. The pCO_2 values ranged between 264-1446 µatm (mean 845 µatm) in summer and between 521-1402 µatm (mean, 904 µatm) in autumn. The dO_2 observations showed values between 4.5-9.5 $mg{\cdot}L^{-1}$ (mean 7.3 $mg{\cdot}L^{-1}$) in summer, and 5.8-8.7 $mg{\cdot}L^{-1}$ (mean, 7.7 $mg{\cdot}L^{-1}$) in autumn, respectively. Although, the mean dO_2 levels were almost identical in two seasons, dO_2 levels were about

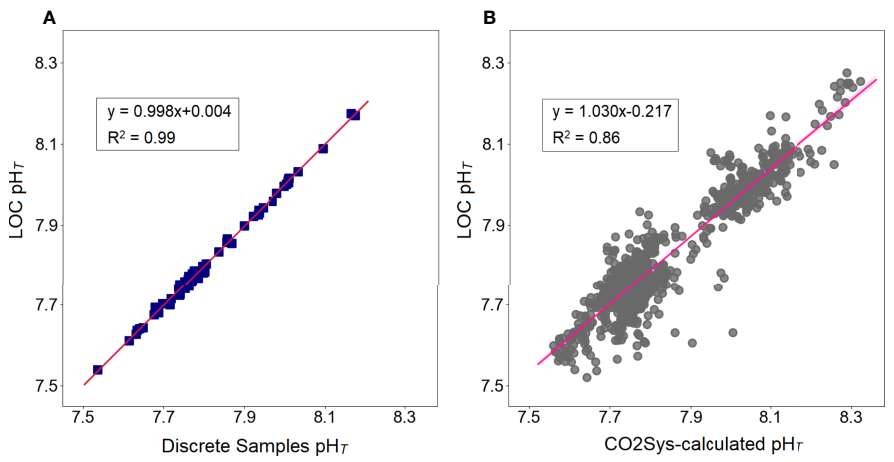

FIGURE 2 | Linear regression fits between all summer and autumn pH_T values obtained from **(A)** discrete water samples *vs* LOC sensor (data: blue squares, linear fit; solid red line, n=65), and **(B)** CO2Sys-calculation *vs* LOC sensor (data: grey circles, linear fit; solid pink line, n=978).

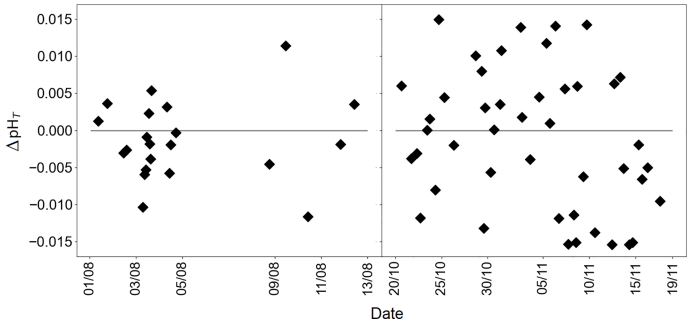

FIGURE 3 | The residuals of ΔpH_T (LOC sensor-discrete water samples) over the duration of summer and autumn deployments, respectively.

TABLE 2 | Summary statistics for in situ pHT and ancillary data from summer and autumn deployments.

Parameter	Summer	Autumn	Parameter	Summer	Autumn
T (°C)	22.1	11.5	**dO_2 (mg·L^{-1})**	7.3	7.7
Mean	18.1-24.2	8.7-14.1	Mean	4.5-9.5	5.8-8.7
Min-Max	6.1	5.4	Min-Max	5	2.9
ΔT	1,325	6,483	ΔdO_2	1,170	6,477
n			n		
S	15.7	20.7	**NO_3^-(μM)**	0.31	2.09
Mean	13.2-18.0	19.6-21.8	Mean	0.08-0.81	0.84-3.83
Min-Max	4.8	2.2	Min-Max	0.73	2.99
ΔS	1,325	6,483	ΔNO_3^-	32	75
n			n		
pH_T (Sensor)	7.954	7.742	**PO_4^{3-} (μM)**	0.47	1.30
Mean	7.520-8.275	7.560-7.932	Mean	0.16-1.51	1.11-1.55
Min-Max	0.755	0.372	Min-Max	1.35	0.44
ΔpH_T	346	632	ΔPO_4^{3-}	32	75
n			n		
pCO_2(μatm)	845	904	**SiO_4^{4-}(μM)**	9.12	24.3
Mean	264-1446	521-1402	Mean	1.7-23.3	19.9-28.6
Min-Max	1182	881	Min-Max	21.6	8.7
ΔpCO_2	53,293	41,756	ΔSiO_4^{4-}	32	75
n			n		

Δ refers to the difference between maximum and minimum values, n is the sample size.

two times more dynamic in summer (ΔdO_2 was 5 mg·L^{-1} in summer and 2.9 mg·L^{-1} in autumn, respectively).

Discretely analyzed samples of nutrients exhibited that NO_3^- concentrations in summer were depleted with values between 0.08 and 0.81 μM (mean 0.31 μM), and was followed by an increase in autumn, with concentrations between 0.84 and 3.83 μM (mean 2.09 μM). Mean PO_4^{3-} and SiO_4^{-4} concentrations were also higher in autumn. In summer, the concentration range for PO_4^{3-} was 0.16-1.51 μM (mean 0.47 μM) and for SiO_4^{-4} 1.7-23.3 μM (mean 9.12 μM), whilst in autumn PO_4^{3-} concentrations varied from 1.1 to 1.55 μM (mean 1.30 μM) and SiO_4^{-4} from 19.9 to 28.6 μM (mean 24.3 μM). The wind speed was maximum 11 m·s^{-1} in summer (mean 3.2 m·s^{-1}), and 13 m·s^{-1} in autumn (mean 4.1 m·s^{-1}).

Diel variations of seawater temperature, salinity, pH_T, and ancillary variables (pCO_2, A_T, dO_2, nutrients, water level, solar irradiance and wind speed) obtained during the first deployment in summer 2018 are presented in **Figure 4**. A total of 346 LOC sensor measurements and 21 discrete seawater samples for pH and 32 for nutrients were collected from August 1 to August 13 on the GEOMAR pontoon facility in Kiel Fjord. The 3-day gap in the dataset, between August 5 and 8, was associated with an electrical failure of the power supply to the sensor. The ranges of all variables and the number of samples measured are presented in **Table 2**.

Co-located deployment of independent sensors facilitated the validation of the time-series data at a higher spatial and temporal resolution than can be achieved by analysis of discrete samples (Martz et al., 2015). Considering the high diel variability in temperature, salinity, pH_T, and the ancillary data presented in **Figure 4**, there was a clear difference between the waters sampled at the beginning and end of the deployment. At the beginning of the deployment period until about August 9, 2018, it can be stated that there was not much activity in the water, referring to tidal ranges (difference between high tide and low tide) below 0.3 m and relatively stable ancillary data.

A rapid decrease in pH_T from 8.249 to 7.573 (determined by the LOC sensor), increase in pCO_2 from 292 to 1029 μatm and

decrease in dO_2 from 9.2 to 5.4 mg·L^{-1} was observed within 24 h from August 9 to 10, 2018, corresponded to a heavy storm event with wind speeds up to 11 m·s^{-1}. This event coincided with the extreme weather alert from the German Weather Service (https://www.dwd.de/DE/presse/pressemitteilungen/DE/2018/20180830_deutschlandwetter_august_news.html). A typical tidal range for the Fjord is ±1 m (Geißler et al., 2021). The water level, temperature and salinity measurements presented in **Figure 4** illustrate the impact of the storm on the sampled waters. The surface waters of the Kiel Fjord are characterized by enhanced temperature and low salinity, as opposed to the bottom waters of low temperature and high salinity. Shifts in seawater temperature (approximately 3°C decrease) and salinity (approximately 2 units increase) values were observed during the storm. Nutrients were in a trend consistent with pCO_2, and both increased in response to increased wind speed and decreased temperatures (**Figure 4**). Enhanced biological activity was evidenced as while nutrients and pCO_2 were increasing, A_T and dO_2 were in decreasing trend. The *in situ* determined pH_T values were a reflection of pCO_2 and dO_2 levels.

Anomalous characteristics of the Baltic Sea waters with respect to major ions and hence alkalinity do not allow a straightforward calculation of alkalinity using salinity that applies to all regions of the Baltic Sea in general (Hammer et al., 2014; Müller et al., 2016). Müller et al. (2016) describes the temporal alkalinity trends in the Baltic Sea using long-term historical datasets and shows the relationship between alkalinity and salinity at four different basins. Instead, we have theoretically calculated A_T using *in situ* salinity data from our deployments and the equation for the Atlantic waters (0°C<T<20°C, 31<S<37) from Lee et al. (2006) to compute pH_T using CO2Sys and have a view of A_T values for our study site. During the summer deployment, salinity-derived A_T values ranged between 2205 and 2427 µmol·kg^{-1} with a mean of 2267 µmol·kg^{-1}. Although the salinity-derived A_T values are not exactly suitable for our study area, when the pH_T values calculated using these A_T and *in situ* pCO_2 data are compared with the sensor pH_T values, a significant relationship is seen (**Figure 2B**).

The second deployment at the same location took place in autumn 2018, from October 20 to November 19, during which

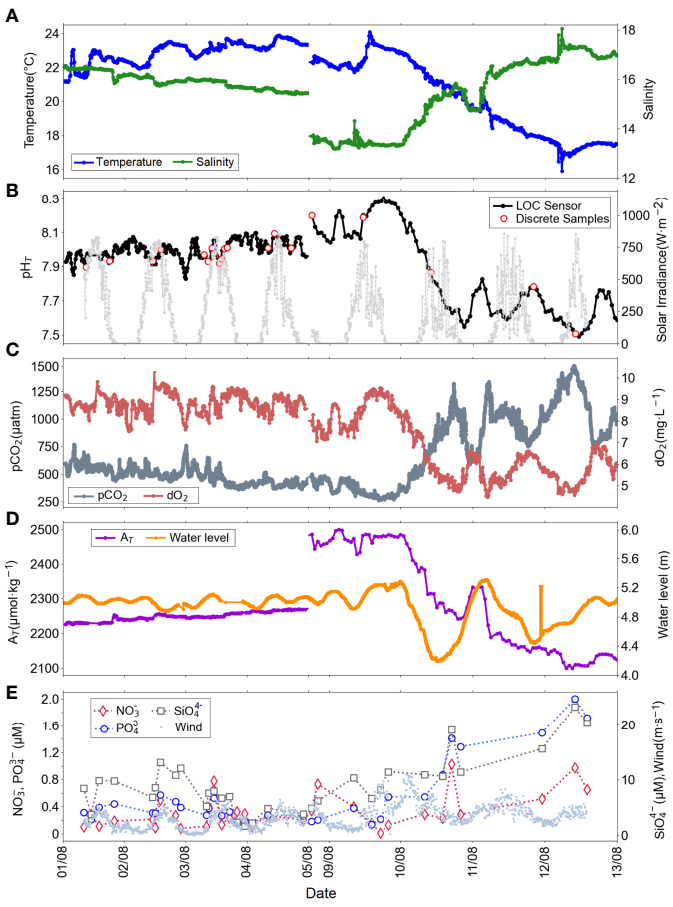

FIGURE 4 | Diel variations of **(A)** *in situ* temperature (blue), *in situ* salinity (green), **(B)** *in situ* pH_T (black: LOC sensor, red circles: discrete water samples , yellow circle: outliers), solar irradiance (light grey), **(C)** *in situ* pCO_2 (dark grey), *in situ* dO_2 (coral), **(D)** salinity-derived A_T (purple), water height (orange), and **(E)** NO_3^- (red diamond), PO_4^{3-}, (blue circles), SiO_4^{-4} (grey squares), and wind speed (pale blue dots) with multiple sensors deployed at the GEOMAR pontoon in Kiel Fjord in summer 2018, from 01.08 to 05.08 and from 08.08 to 13.08.

632 LOC sensor measurements were conducted, and discrete seawater samples for discrete seawater samples for pH (n=44) and for nutrients (n=75) were collected. Diel variations of the seawater pH_T and ancillary data are shown in **Figure 5** and the corresponding value ranges are provided in **Table 2**. The tide gauge water level measurements at Kiel Fjord corresponding to our measuring period indicated that during a heavy storm (wind speed up to ca. 13 m·s^{-1}, **Figure 5E**), the water level increased by about 1 m (from 4.46 to 5.46 m, **Figure 5D**).

During the autumn deployment a further notable weather event occurred starting from October 26th, a storm flood approached at the sampling site, followed by successive winds (speed >10 m·s^{-1}) for about 3 days. Over the same period, daily rain intensities (precipitation) of ca. 10 mm were captured, which is a threshold of a heavy rainfall event for Germany (Deumlich and Gericke, 2020), and reductions in water temperature and salinity of about 2 units were observed with additional responses in pH_T, pCO_2, dO_2 and NO_3^- levels. Strongly variable increases in pH_T values were observed, presented in the yellow circle in **Figure 5B**, and were not included in **Table 2**. This was likely due to the variations in the physical conditions of the fjord waters with winds and tides. The in line filter of the LOC sensor was changed on November 1, 2018, to avoid possible clogging after dynamic water conditions. The gaps (couple of hours) in the LOC sensor dataset between October 25 and 26, as well as November 11 and 12, were related to the power cuts.

The salinity-derived A_T values ranged between 2075 and 2130 µmol·kg^{-1} with a mean of 2099 µmol·kg^{-1} in autumn, much lower than those reported in summer. Compared to the first deployment (**Figure 4**), the time series data presented in **Figure 5** were relatively uniform with small differences between maximum and minimum values of all parameters (as indicated by low Δ values, **Table 2**). An increase in NO_3^- concentrations, from 1.70 to 3.83 µM, was noticed over a one-day period, between November 5 and 6, 2018. The dO_2 levels decreased from 8.5 to 7.9 mg·L^{-1}, whilst pCO_2 levels increased from 704 to 961 µatm. The acidification

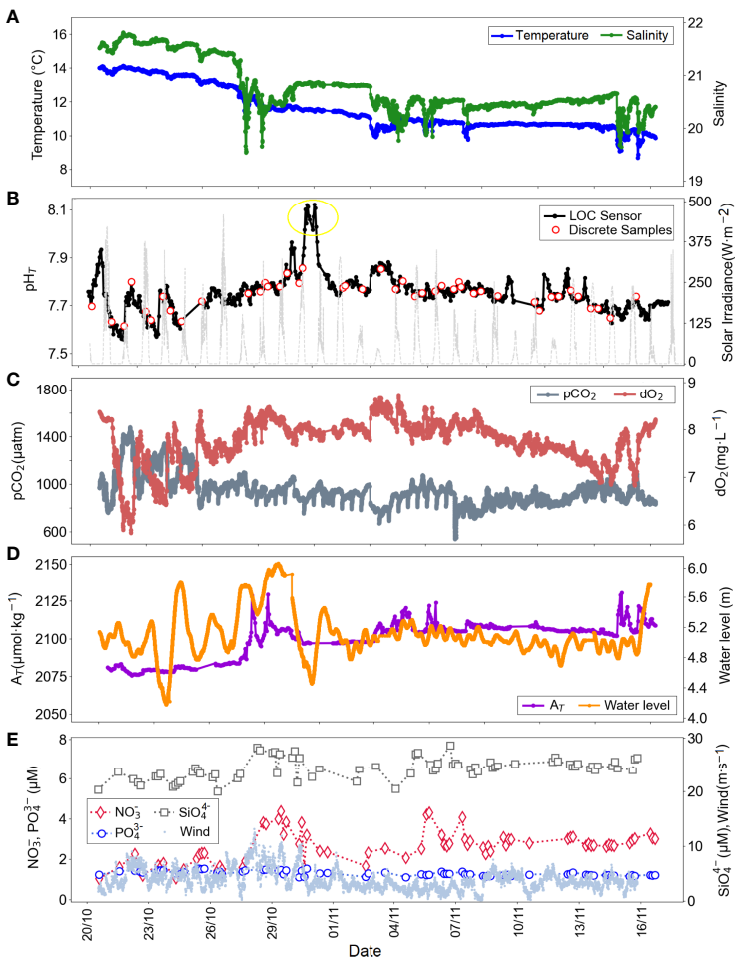

FIGURE 5 | Diel variations of **(A)** *in situ* temperature (blue), *in situ* salinity (green), **(B)** *in situ* pH_T (black: LOC sensor, red circles: discrete water samples, yellow circle: outliers), solar irradiance (light grey), **(C)** *in situ* pCO_2 (dark grey), *in situ* dO_2 (coral), **(D)** salinity-derived A_T (purple), water height (orange), and **(E)** NO_3^- (red diamond), PO_4^{3-}, (blue circles), SiO_4^{-4} (grey squares), and wind speed (pale blue dots) with multiple sensors deployed at the GEOMAR pontoon in Kiel Fjord in autumn 2018, from October 20 to November 19.

process was evidenced with decreasing pH values from 7.858 to 7.752. This event can be ascribed to supply of subsurface waters enriched in DIC due to organic matter respiration process (see also section 3.3).

Carbonate Chemistry Dynamics in Kiel Fjord

Estuarine and coastal waters feature complex hydrological conditions, often including strong variations in surface salinity (Castelao et al., 2010). Carbonate chemistry in coastal waters is regulated by variety of factors, including biological metabolic (photosynthesis, respiration, and calcium carbonate precipitation or dissolution), and physical processes (ocean currents, tide, weather conditions) (Kristiansen et al., 2001; Feely et al., 2010; Stokowski et al., 2020; Huang et al., 2021). A change in the mass balance of the carbonate system or thermodynamic conditions of the waters affect the surface pCO_2 levels, consequently the pH dynamics (Dai et al., 2009).

pH_T and ancillary data, presented in this study, exhibited clear diel variations (**Figures 4**, **5**), and the patterns were different in the two seasons, suggesting that distinct internal processes may be involved in regulating these variations. At our deployment site, observations indicated that in the nearshore surface waters of Kiel Fjord were colder, saltier, and more acidic in autumn compared to summer (**Figure 6**). The ΔpH_T was 0.372 units in autumn and 0.755 units in summer, respectively.

pH, pCO_2 and dO_2 are important indicators for characterizing water masses and biological processes (Orr et al., 2005; Staudinger et al., 2018). An increase in dO_2 concentrations corresponded to an increase in pH and decrease in pCO_2 levels in waters, due to enhanced photosynthetic activity of algae. The mean differences in dO_2 between summer and autumn can also be attributed to the fact that the effect of wind mixing on the water was sharper in our summer distributions, as the waters are generally not well mixed in the summer. The increase in nutrient concentrations and pCO_2 while the dO_2 decreases are evidence of the biological life in the environment. The pH time-series data mirrors that of pCO_2 and dO_2, when fit to a linear regression yielded $r^2 = 0.85$ and $r^2 = 0.77$ in summer and yielded $r^2 = 0.46$ and $r^2 = 0.70$ in autumn, respectively (**Figure 7**). Besides, pCO_2 data can be considered as a form of validation of the pH data, as *in situ* measurements were conducted using two different sensors; CONTROS HydroC and LOC.

The observed Redfield ratios, defining the stoichiometry of the photosynthesis and respiration reactions (Redfield et al., 1963), are shown in **Table 3**. The molar ratios between carbon, nitrogen, and phosphorus from simultaneous measurements on the deployment site indicated that the C:N ratio was largely above the proposed Redfield ratio of 106C:16N, which may be related to N loss processes due to denitrification (Gruber, 2008). The N:P ratio in our data was below the Redfield ratio of 16N:1P, which may again be related to N loss through denitrification and additional benthic P supply from anoxic sediments (Lenton and Watson, 2000).

Our data from the Kiel Fjord shows strongly elevated *in situ* pCO_2 (maximum of 1420 µatm) levels, even higher than reported for other estuaries. For example the Polish Oder Estuary which also drains into the Baltic Sea has reported pCO_2 values of<1200 µatm (Stokowski et al., 2020). Higher CO_2 levels were related to nutrient enrichment in the system (**Figure 8**), with respiration resulting in O_2 consumption and CO_2 production (**Figures 4**, **5**).

The physical mixing and enhanced remineralization of organic substances in estuaries, promoted by high nutrient loads from land, determine the chemical composition of the system (Bauer et al., 2013; Stokowski et al., 2020). While it is beyond the scope of this study to precisely quantify the intensity of photosynthesis/respiration processes, studies from different estuaries have suggested that intensity levels of biological activities are modulated by wind-driven inputs of nutrients from subsurface waters (Gazeau et al., 2005; Saderne et al., 2013; Li et al., 2020).

Given our *in situ* data and the main biological and physical drivers of the carbonate chemistry of the estuarine systems, the carbonate system in Kiel Fjord is regulated by i) respiration, and ii) wind-driven mixing. During the deployment periods storm

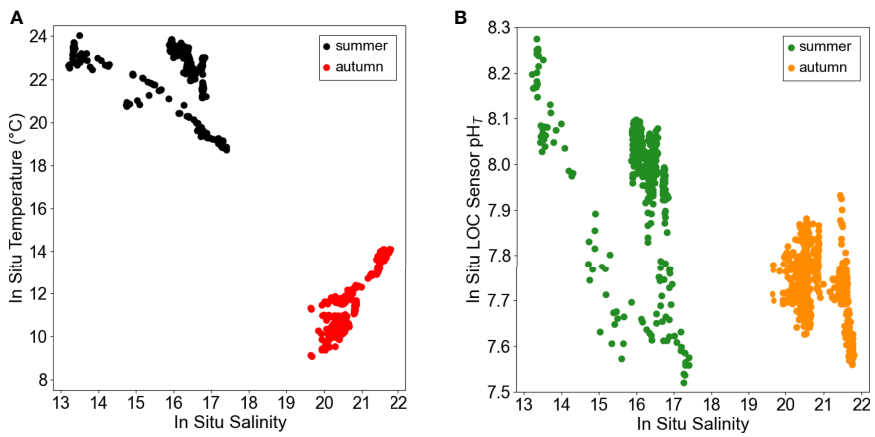

FIGURE 6 | *In situ* **(A)** temperature-salinity and **(B)** pH_T-salinity diagram of the period investigated, illustrating different hydrological periods in summer (black, green circles) and autumn (red, orange circles).

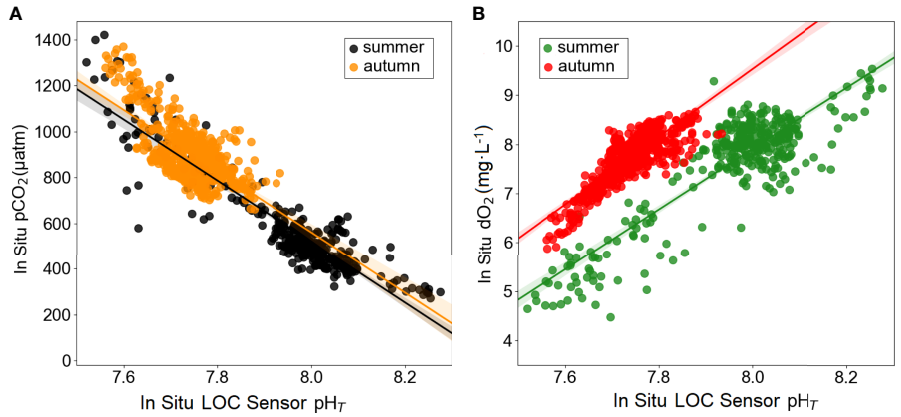

FIGURE 7 | Linear regression (solid lines) plots between **(A)** pCO_2 and pH_T (black circles present the data from the summer time-series *in situ* data presented in **Figure 4**, linear fit yielded $r^2 = 0.85$ (n=346) and orange circles present the data from the autumn time-series *in situ* data presented in **Figure 5**, linear fit yielded $r^2 = 0.46$ (n=632), and **(B)** dO_2 and pH_T (green circles present the data from the summer time-series *in situ* data presented in **Figure 4**, linear fit yielded $r^2 = 0.77$ (n=346) and red circles present the data from the autumn time-series *in situ* data presented in **Figure 5**, linear fit yielded $r^2 = 0.70$ (n=632).

Table 3 | Molar ratios of C, N and P derived from simultaneous observations during deployment periods.

	C:N RatioSummer	N:P RatioSummer	C:N RatioAutumn	N:P RatioAutumn
Min	17.6	0.213	10.3	0.650
Max	224	2.64	48.2	3.07
Mean	86.9	0.798	21.8	1.65

events were captured, in which subsurface waters (with enhanced pCO_2 and nutrient levels) were transferred to the surface, evidenced by temperature and salinity observations.

CONCLUSION

Understanding spatial and temporal changes in pH in association with environmental variables is essential for a sustainable management of marine systems. Hydrodynamic and biogeochemical processes in coastal estuaries change rapidly from minutes to days, triggering acidification in the system (Xu et al., 2017; Wright-Fairbanks et al., 2020). Those sudden changes often cannot be resolved through sampling and analyses of discrete water samples. The automated real-time observation of carbonate chemistry dynamics with sensors like LOC offer a potentially substantial improvement in that regard. While the performances of the LOC sensor for high-resolution spectrophotometric pH

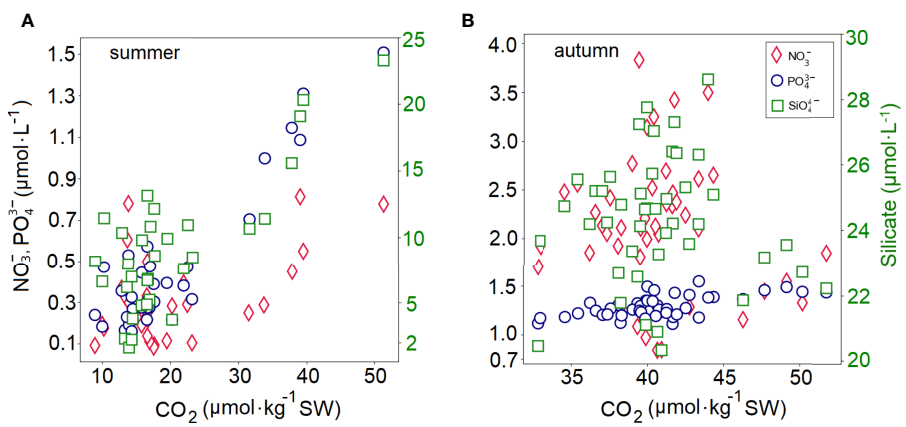

FIGURE 8 | Dynamics of *in situ* concentration of dissolved CO_2 gas in the water sample (calculated using the CO2Sys) vs nutrients during the **(A)** summer and **(B)** autumn deployment.

measurements has been demonstrated in surface waters of shelf seas with salinities above 24 (Rérolle et al., 2018; Yin et al., 2021), this is the first report on deployments of the sensor in dynamic estuarine waters (S<20).

Our study shows the effects of respiration and wind-driven mixing of water masses leading to consecutive impacts on the carbonate chemistry of the Kiel Fjord. The presented *in situ* data from observations conducted within a period of six weeks in two seasons (summer and autumn) showed the suitability of the LOC pH sensor for revealing the strong dynamics in highly dynamic estuarine waters on a fine temporal scale. The applicability of the sensor is broad, it was integrated on a Seaglider (iRobot/Kongsberg) (Possenti et al., 2021), on an Autosub Long Range AUV (Yin et al., 2021), and on an ROV (Monk et al., 2021). The unique depth rating (6000 m), low power and reagent consumption, low cost, high portability, and ease to use without calibration for long-term monitoring make the LOC sensor a good choice for autonomous pH observations on various monitoring platforms. Work is currently underway for integration of the LOC pH sensor on other AUVs (pers. comm. Socratis Loucaides). The measurement frequency (~8 min) is the main weakness of the sensor when deployed on fast-moving and profiling platforms such as gliders and floats. Future works should focus on optimizing the measurement duration of the sensor to achieve better performance on such platforms.

DATA AVAILABILITY STATEMENT

The raw data supporting the conclusions of this article will be made available by the authors, without undue reservation.

AUTHOR CONTRIBUTIONS

MN performed the laboratory and field work, statistical analysis and data visualization. ME performed the installation of the sensors on the deployment platform. MN wrote the first draft of the manuscript. All authors contributed to the article and approved the submitted version.

FUNDING

This study was supported by funding to EA from the European Union's Horizon 2020 Research and Innovation Program under the AtlantOS program, grant agreement No. 633211. EA acknowledges funding for the OCEANSensor project as part of the MARTERA Programme and financed by the German Federal Ministry of Economic Affairs and Energy (BMWi; Funding Agreement 03SX459A).

ACKNOWLEDGMENTS

The authors thank Class Hiebenthal and Christian Begler for providing the post-processed pCO_2 data of the CONTROS HydroC CO_2 sensor, and Björn Buchholz for assistance with the deployment facility on a floating pontoon at GEOMAR Helmholtz Centre for Ocean Research (Kiel, Germany). The authors also thank Maria Martinez-Cabanas and Felix Geissler for their assistance with the collection of discrete water samples.

REFERENCES

Aßmann, S., Frank, C. and Körtzinger, A. (2011). Spectrophotometric High-Precision Seawater pH Determination for Use in Underway Measuring Systems. *Ocean. Sci.* 7, 597–607. doi: 10.5194/os-7-597-2011

Bauer, J. E., Cai, W. J., Raymond, P. A., Bianchi, T. S., Hopkinson, C. S. and Regnier, P. A. G. (2013). The Changing Carbon Cycle of the Coastal Ocean. *Nature* 504, 61–70. doi: 10.1038/nature12857

Becker, S., Aoyama, M., Woodward, E. M. S., Bakker, K., Coverly, S., Mahaffey, C., et al. (2019). GO-SHIP Repeat Hydrography Nutrient Manual: The Precise and Accurate Determination of Dissolved Inorganic Nutrients in Seawater, Using Continuous Flow Analysis Methods. *Front. Marine. Sci.* 7 (581790), 1–15. doi: 10.3389/fmars.2020.581790

Bellerby, R. G. J., Olsen, A., Johannessen, T. and Croot, P. (2002). A High Precision Spectrophotometric Method for on-Line Shipboard Seawater pH Measurements: The Automated Marine pH Sensor (AMpS). *Talanta* 56, 61–69. doi: 10.1016/S0039-9140(01)00541-0

Blaisdell, J., Thalmann, H. L., Klajbor, W., Zhang, Y., Miller, J. A., Laurel, B. J., et al. (2021). A Dynamic Stress-Scape Framework to Evaluate Potential Effects of Multiple Environmental Stressors on Gulf of Alaska Juvenile Pacific Cod. *Front. Mar. Sci.* 8, 656088. doi: 10.3389/fmars.2021.656088

Bresnahan, P. J., Martz, T. R., Takeshita, Y., Johnson, K. S. and LaShomb, M. (2014). Best Practices for Autonomous Measurement of Seawater pH With the Honeywell Durafet. *Methods Oceanogr.* 9, 44–60. doi: 10.1016/j.mio.2014.08.003

Bresnahan, P. J., Takeshita, Y., Wirth, T., Martz, T. R., Cyronak, T., Albright, R., et al. (2021). Autonomous *In Situ* Calibration of Ion-Sensitive Field Effect Transistor pH Sensors. *Limnol. Oceanogr. Methods*. 19, 132–144. doi: 10.1002/lom3.10410

Carstensen, J., Chierici, M., Gustafsson, B. G. and Gustafsson, E. (2018). Long-Term and Seasonal Trends in Estuarine and Coastal Carbonate Systems. *Global Biogeochem. Cycles.* 32, 497–513. doi: 10.1002/2017GB005781

Castelao, R., Glenn, S. and Schofield, O. (2010). Temperature, Salinity, and Density Variability in the Central Middle Atlantic Bight. *J. Geophys. Res. Ocean.* 115, 1–14. doi: 10.1029/2009JC006082

Clarke, J. S., Achterberg, E. P., Rérolle, V. M. C., Abi Kaed Bey, S., Floquet, C. F. A. and Mowlem, M. C. (2015). Characterisation and Deployment of an Immobilised pH Sensor Spot Towards Surface Ocean pH Measurements. *Anal. Chim. Acta* 897, 69–80. doi: 10.1016/j.aca.2015.09.026

Clayton, T. D. and Byrne, R. H. (1993). Spectrophotometric Seawater pH Measurements: Total Hydrogen Ion Concentration Scale Calibration of M-Cresol Purple and at-Sea Results. *Deep. Res.* 40, 2115–2129. doi: 10.1016/0967-0637(93)90048-8

Dai, M., Lu, Z., Zhai, W., Chen, B., Cao, Z., Zhou, K., et al. (2009). Diurnal Variations of Surface Seawater pCO2 in Contrasting Coastal Environments. *Limnol. Oceanogr.* 54, 735–745. doi: 10.4319/lo.2009.54.3.0735

DeGrandpre, M. D., Spaulding, R. S., Newton, J. O., Jaqueth, E. J., Hamblock, S. E., Umansky, A. A., et al. (2014). Considerations for the Measurement of Spectrophotometric pH for Ocean Acidification and Other Studies. *Limnol. Oceanogr. Methods* 12, 830–839. doi: 10.4319/lom.2014.12.830

Deumlich, D. and Gericke, A. (2020). Frequency Trend Analysis of Heavy Rainfall Days for Germany. *Water* 12, 1–29. doi: 10.3390/w12071950

Dickson, A. G., Sabine, C. L. and Christian, J. R. (2007). *Guide to Best Practices for Ocean CO2 Measurements*. Available at: http://aquacomm.fcla.edu/1443/.

Doney, S. C., Busch, D. S., Cooley, S. R. and Kroeker, K. J. (2020). The Impacts of Ocean Acidification on Marine Ecosystems and Reliant Human Communities. *Annu. Rev. Environ. Resour.* 45, 83–112. doi: 10.1146/annurev-environ-012320-083019

Dore, J. E., Lukas, R., Sadler, D. W., Church, M. J. and Karl, D. M. (2009). Physical and Biogeochemical Modulation of Ocean Acidification in the Central North Pacific. *Proc. Natl. Acad. Sci. U.S.A.* 106, 12235–12240. doi: 10.1073/pnas.0906044106

Douglas, N. K. and Byrne, R. H. (2017). Spectrophotometric pH Measurements From River to Sea: Calibration of mCP for $0 \leq S \leq 40$ and $278.15 \leq T \leq 308.15$ K. *Mar. Chem.* 197, 64–69. doi: 10.1016/j.marchem.2017.10.001

Fassbender, A., Orr, J. and Dickson, A. (2021). Technical Note: Interpreting pH Changes. *Biogeosciences* 18, 1407 –1415. doi: 10.5194/bg-18-1407-2021

Feely, R. A., Alin, S. R., Newton, J., Sabine, C. L., Warner, M., Devol, A., et al. (2010). The Combined Effects of Ocean Acidification, Mixing, and Respiration on pH and Carbonate Saturation in an Urbanized Estuary. *Estuar. Coast. Shelf. Sci.* 88, 442–449. doi: 10.1016/j.ecss.2010.05.004

Feely, R. A., Doney, S. C. and Cooley, S. R. (2009). Ocean Acidification: Present Conditions and Future Changes in a High-CO2 World. *Oceanography* 22, 36–47. doi: 10.5670/oceanog.2009.95

Fietzek, P., Fiedler, B., Steinhoff, T. and Körtzinger, A. (2014). *In Situ* Quality Assessment of a Novel Underwater Pco2 Sensor Based on Membrane Equilibration and NDIR Spectrometry. *J. Atmos. Ocean. Technol.* 31, 181–196. doi: 10.1175/JTECH-D-13-00083.1

Floquet, C. F. A., Sieben, V. J., Milani, A., Joly, E. P., Ogilvie, I. R. G., Morgan, H., et al. (2011). Nanomolar Detection With High Sensitivity Microfluidic Absorption Cells Manufactured in Tinted PMMA for Chemical Analysis. *Talanta* 84, 235–239. doi: 10.1016/j.talanta.2010.12.026

Fox, L., Stukins, S., Hill, T. and Miller, C. G. (2020). Quantifying the Effect of Anthropogenic Climate Change on Calcifying Plankton. *Sci. Rep.* 10, 1–9. doi: 10.1038/s41598-020-58501-w

Friedlingstein, P., O'Sullivan, M., Jones, M. W., Andrew, R. M., Hauck, J., Olsen, A., et al. (2020). Global Carbon Budget 2020. *Earth Syst. Sci. Data* 12, 3269–3340. doi: 10.5194/essd-12-3269-2020

Gazeau, F., Borges, A. V., Barrón, C., Duarte, C. M., Iversen, N., Middelburg, J. J., et al. (2005). Net Ecosystem Metabolism in a Micro-Tidal Estuary (Randers Fjord, Denmark): Evaluation of Methods. *Mar. Ecol. Prog. Ser.* 301, 23–41. doi: 10.3354/meps301023

Geißler, F., Achterberg, E. P., Beaton, A. D., Hopwood, M. J., Esposito, M., Mowlem, M. C., et al. (2021). Lab-On-Chip Analyser for the *in Situ* Determination of Dissolved Manganese in Seawater. *Sci. Rep.* 11, 1–13. doi: 10.1038/s41598-021-81779-3

Grand, M. M., Clinton-Bailey, G. S., Beaton, A. D., Schaap, A. M., Johengen, T. H., Tamburri, M. N., et al. (2017). A Lab-On-Chip Phosphate Analyzer for Long-Term *In Situ* Monitoring at Fixed Observatories: Optimization and Performance Evaluation in Estuarine and Oligotrophic Coastal Waters. *Front. Mar. Sci.* 4, 255. doi: 10.3389/fmars.2017.00255

Gruber, N. (2008). "The Marine Nitrogen Cycle: Overview and Challenges," in *Nitrogen in the Marine Environment* (Netherlands: Elsevier Inc), 1–50. doi: 10.1016/B978-0-12-372522-6.00001-3

Guinotte, J. M. and Fabry, V. J. (2008). Ocean Acidification and its Potential Effects on Marine Ecosystems. *Ann. N. Y. Acad. Sci.* 1134, 320–342. doi: 10.1196/annals.1439.013

Hall, E. R., Wickes, L., Burnett, L. E., Scott, G. I., Hernandez, D., Yates, K. K., et al. (2020). Acidification in the U.S. Southeast: Causes, Potential Consequences and the Role of the Southeast Ocean and Coastal Acidification Network. *Front. Mar. Sci.* 7, 548. doi: 10.3389/fmars.2020.00548

Hammer, K., Schneider, B. and Kuli, K. (2014). Precision and Accuracy of Spectrophotometric pH Measurements at Environmental Conditions in the Baltic Sea. *Estuar. Coast. Shelf. Sci.* 146, 24–32. doi: 10.1016/j.ecss.2014.05.003

Hoffmann, L. J., Breitbarth, E., Boyd, P. W. and Hunter, K. A. (2012). Influence of Ocean Warming and Acidification on Trace Metal Biogeochemistry. *Mar. Ecol. Prog. Ser.* 470, 191–205. doi: 10.3354/meps10082

Huang, W. J., Cai, W. J. and Hu, X. (2021). Seasonal Mixing and Biological Controls of the Carbonate System in a River-Dominated Continental Shelf Subject to Eutrophication and Hypoxia in the Northern Gulf of Mexico. *Front. Mar. Sci.* 8, 621243. doi: 10.3389/fmars.2021.621243

Hudson-Heck, E., Liu, X. and Byrne, R. H. (2021). Purification and Physical-Chemical Characterization of Bromocresol Purple for Carbon System Measurements in Freshwaters, Estuaries, and Oceans. *ACS Omega*. 6, 17941–17951. doi: 10.1021/acsomega.1c01579

Hu, X., Pollack, J. B., McCutcheon, M. R., Montagna, P. A. and Ouyang, Z. (2015). Long-Term Alkalinity Decrease and Acidification of Estuaries in Northwestern Gulf of Mexico. *Environ. Sci. Technol.* 49, 3401–3409. doi: 10.1021/es505945p

Ishida, H., Isono, R. S., Kita, J. and Watanabe, Y. W. (2021). Long-Term Ocean Acidification Trends in Coastal Waters Around Japan. *Sci. Rep.* 11, 1–7. doi: 10.1038/s41598-021-84657-0

Jiang, L., Carter, B. R., Feely, R. A., Lauvset, S. K. and Olsen, A. (2019). Surface Ocean pH and Buffer Capacity: Past, Present and Future. *Sci. Rep.* 9, 1–11. doi: 10.1038/s41598-019-55039-4

Johnson, K. S., Jannasch, H. W., Coletti, L. J., Elrod, V. A., Martz, T. R., Takeshita, Y., et al. (2016). Deep-Sea DuraFET: A Pressure Tolerant pH Sensor Designed for Global Sensor Networks. *Anal. Chem.* 88, 3249–3256. doi: 10.1021/acs.analchem.5b04653

Kristiansen, S., Farbrot, T. and Naustvoll, L.-J. (2001). Spring Bloom Nutrient Dynamics in the Oslofjord. *Mar. Ecol. Prog. Ser.* 219, 41–49. doi: 10.3354/meps219041

Kwiatkowski, L., Torres, O., Bopp, L., Aumont, O., Chamberlain, M., R. Christian, J., et al. (2020). Twenty-First Century Ocean Warming, Acidification, Deoxygenation, and Upper-Ocean Nutrient and Primary Production Decline From CMIP6 Model Projections. *Biogeosciences* 17, 3439–3470. doi: 10.5194/bg-17-3439-2020

Lai, C., Degrandpre, M. D., Wasser, B. D., Brandon, T. A., Clucas, D. S., Jaqueth, E. J., et al. (2016). Spectrophotometric Measurement of Freshwater pH With Purified Meta-Cresol Purple and Phenol Red. *Limnol. Oceanogr. Methods* 14, 864–873. doi: 10.1002/lom3.10137

Lai, C., Degrandpre, M. D., Wasser, B. D., Brandon, T. A., Clucas, D. S., Jaqueth, E. J., et al. (2017). Corrigendum Spectrophotometric Measurement of Freshwater pH With Purified Meta-Cresol Purple and Phenol Red. *Limnol. Oceanogr. Methods* 15, 903. doi: 10.1002/lom3.10210

Lee, K., Tong, L. T., Millero, F. J., Sabine, C. L., Dickson, A. G., Goyet, C., et al. (2006). Global Relationships of Total Alkalinity With Salinity and Temperature in Surface Waters of the World's Oceans. *Geophys. Res. Lett.* 33, 1–5. doi: 10.1029/2006GL027207

Lenton, T. M. and Watson, A. J. (2000). Redfield Revisited 1. Regulation of Nitrate, Phosphate, and Oxygen in the Ocean. *Global Biogeochem. Cycles*. 14, 225–248. doi: 10.1029/1999GB900065

Lewis, E. and Wallace, D. W. R. (1998). *Program Developed for CO2 System Calculations* (Oak Ridge National Laboratory). ORNL/ CDIAC-105.

Li, M., Li, R., Cai, W. J., Testa, J. M. and Shen, C. (2020). Effects of Wind-Driven Lateral Upwelling on Estuarine Carbonate Chemistry. *Front. Mar. Sci.* 7, 588465. doi: 10.3389/fmars.2020.588465

Liu, X., Patsavas, M. C. and Byrne, R. H. (2011). Purification and Characterization of Meta-Cresol Purple for Spectrophotometric Seawater pH Measurements. *Environ. Sci. Technol.* 45, 4862–4868. doi: 10.1021/es200665d

Loucaides, S., Rèrolle, V. M. C., Papadimitriou, S., Kennedy, H., Mowlem, M. C., Dickson, A. G., et al. (2017). Characterization of Meta-Cresol Purple for Spectrophotometric pH Measurements in Saline and Hypersaline Media at Sub-Zero Temperatures. *Sci. Rep.* 7, 1–11. doi: 10.1038/s41598-017-02624-0

Martz, T. R., Carr, J. J., French, C. R. and Degrandpre, M. D. (2003). A Submersible Autonomous Sensor for Spectrophotometric pH Measurements of Natural Waters. *Anal. Chem.* 75, 1844–1850. doi: 10.1021/ac020568l

Martz, T. R., Connery, J. G. and Johnson, K. S. (2010). Testing the Honeywell Durafet for Seawater pH Applications. *Limnol. Oceanogr. Methods* 8, 172–184. doi: 10.4319/lom.2010.8.172

Martz, T., Mclaughlin, K. and Weisberg, S. B. (2015). Best Practices for Autonomous Measurement of Seawater pH With the Honeywell Durafet pH Sensor. 1–20.

Mclaughlin, K., Dickson, A., Weisberg, S. B., Coale, K., Elrod, V., Hunter, C., et al. (2017). An Evaluation of ISFET Sensors for Coastal pH Monitoring Applications. *Reg. Stud. Mar. Sci.* 12, 11–18. doi: 10.1016/j.rsma.2017.02.008

Midorikawa, T., Ishii, M., Saito, S., Sasano, D., Kosugi, N., Motoi, T., et al. (2010). Decreasing pH Trend Estimated From 25-Yr Time Series of Carbonate Parameters in the Western North Pacific. *Tellus. Ser. B. Chem. Phys. Meteorol.* 62, 649–659. doi: 10.1111/j.1600-0889.2010.00474.x

Millero, F. J. (2007). The Marine Inorganic Carbon Cycle. *Chem. Rev.* 107, 308–341. doi: 10.1021/cr0503557

Millero, F. J., Woosley, R., Ditrolio, B. and Waters, J. (2009). Effect of Ocean Acidification on the Speciation of Metals in Seawater. *Oceanography* 22, 72–85. doi: 10.5670/oceanog.2009.98

Miller, C. A., Pocock, K., Evans, W. and Kelley, A. L. (2018). An Evaluation of the Performance of Sea-Bird Scientific's SeaFET™ Autonomous pH Sensor: Considerations for the Broader Oceanographic Community. *Ocean. Sci.* 14, 751–768. doi: 10.5194/os-14-751-2018

Monk, S. A., Schaap, A., Hanz, R., Borisov, S. M., Loucaides, S., Arundell, M., et al. (2021). Detecting and Mapping a CO2 Plume With Novel Autonomous pH Sensors on an Underwater Vehicle. *Int. J. Greenh. Gas. Control.* 112, 1–13. doi: 10.1016/j.ijggc.2021.103477

Mosley, L. M., Husheer, S. L. G. and Hunter, K. A. (2004). Spectrophotometric pH Measurement in Estuaries Using Thymol Blue and M-Cresol Purple. *Mar. Chem.* 91, 175–186. doi: 10.1016/j.marchem.2004.06.008

Müller, J. D. and Rehder, G. (2018). Metrology of pH Measurements in Brackish Waters — Part 2: Experimental Characterization of Purified Meta-Cresol Purple for Spectrophotometric pHT Measurements. *Front. Mar. Sci.* 5, 177. doi: 10.3389/fmars.2018.00177

Müller, J. D., Schneider, B. and Rehder, G. (2016). Long-Term Alkalinity Trends in the Baltic Sea and Their Implications for CO2-Induced Acidification. *Limnol. Oceanogr.* 61, 1984–2002. doi: 10.1002/lno.10349

Nikulina, A., Polovodova, I. and Schönfeld, J. (2008). Foraminiferal Response to Environmental Changes in Kiel Fjord, SW Baltic Sea. *eEarth* 3, 37–49. doi: 10.5194/ee-3-37-2008

Orr, J. C., Fabry, V. J., Aumont, O., Bopp, L., Doney, S. C., Feely, R. A., et al. (2005). Anthropogenic Ocean Acidification Over the Twenty-First Century and its Impact on Calcifying Organisms. *Nature* 437, 681–686. doi: 10.1038/nature04095

Perez, I. M., Sansalvador, D. V., Fay, C. D., Cleary, J., Nightingale, A. M., Mowlem, M. C., et al. (2016). Autonomous Reagent-Based Microfluidic pH Sensor Platform. *Sensors. Actuators. B. Chem.* 225, 369–376. doi: 10.1016/j.snb.2015.11.057

Pierrot, D., Lewis, E. and Wallace, D. W. R. (2006). *MS Excel Program Developed for CO2 System Calculations. Carbon Dioxide Information Analysis Center* (US: Oak Ridge National Laboratory). doi: 10.3334/CDIAC/otg.CO2SYSXLSCD

Possenti, L., Humphreys, M. P., Bakker, D. C. E., Cobas-García, M., Fernand, L., Lee, G. A., et al. (2021). Air-Sea Gas Fluxes and Remineralization From a Novel Combination of pH and O2 Sensors on a Glider. *Front. Mar. Sci.* 8, 696772. doi: 10.3389/fmars.2021.696772

Redfield, A. C., Ketchum, B. H. and Richards, F. A. (1963). "The Influence of Organisms on the Composition of the Sea Water," in *Sea*, vol. 2 . Ed. Hill, M. N. (New York, London: Intersci. Publ), 26–77.

Rérolle, V. M. C., Achterberg, E. P., Ribas-Ribas, M., Kitidis, V., Brown, I., Bakker, D. C. E., et al. (2018). High Resolution pH Measurements Using a Lab-On-Chip Sensor in Surface Waters of Northwest European Shelf Seas. *Sensors* 18, 1–23. doi: 10.3390/s18082622

Rérolle, V. M. C., Floquet, C. F. A., Harris, A. J. K., Mowlem, M. C., Bellerby, R. R. G. J. and Achterberg, E. P. (2013). Development of a Colorimetric Microfluidic pH Sensor for Autonomous Seawater Measurements. *Anal. Chim. Acta* 786, 124–131. doi: 10.1016/j.aca.2013.05.008

Rérolle, V. M. C., Floquet, C. F. A., Mowlem, M. C., Bellerby, R. R. G. J., Connelly, D. P. and Achterberg, E. P. (2012). Seawater-pH Measurements for Ocean-Acidification Observations. *Trends Anal. Chem.* 40, 146–157. doi: 10.1016/j.trac.2012.07.016

Rérolle, V., Ruiz-Pino, D., Rafizadeh, M., Loucaides, S., Papadimitriou, S., Mowlem, M., et al. (2016). Measuring pH in the Arctic Ocean: Colorimetric Method or SeaFET? *Methods Oceanogr.* 17, 32–49. doi: 10.1016/j.mio.2016.05.006

Riebesell, U., Fabry, V., Hansson, L., and Gattuso, J. P. (2010). *Guide to Best Practices for Ocean Acidification Research and Data Reporting* (Brussels, Belgium: Publications Office of the European Union).

Robert-Baldo, G. L., Morris, M. J. and Byme, R. H. (1985). Spectrophotometric Determination of Seawater pH Using Phenol Red. *Anal. Chem.* 57, 2564–2567. doi: 10.1021/ac00290a030

Sabine, C. L., Feely, R. A., Gruber, N., Key, R. M., Lee, K., Bullister, J. L., et al. (2004). The Oceanic Sink for Anthropogenic Co2. *Sci. (80-.).* 305, 367–371. doi: 10.1126/science.1097403

Saderne, V., Fietzek, P. and Herman, P. M. J. (2013). Extreme Variations of Pco2 and pH in a Macrophyte Meadow of the Baltic Sea in Summer: Evidence of the Effect of Photosynthesis and Local Upwelling. *PloS One* 8 , 1–8. doi: 10.1371/journal.pone.0062689

Sastri, A. R., Christian, J. R., Achterberg, E. P., Atamanchuk, D., Buck, J. J. H., Bresnahan, P., et al. (2019). Perspectives on *In Situ* Sensors for Ocean Acidification Research. *Front. Mar. Sci.* 6, 653. doi: 10.3389/fmars.2019.00653

Schories, D., Selig, U., Schubert, H., Jegzentis, K., Mertens, M., Schubert, M., et al. (2006). Küstengewässer-Klassifizierung deutsche Ostsee nach EU-WRRL. Tl. A Äußere Küstengewässer. Forschungsbericht.

Sea-Bird Electronics Inc. Available at: http://satlantic.com/seafet (Accessed January 11, 2021). Sea-Bird Scientific, USA. SeaFETTM V2 and SeapHOxTM V2 User manual. Sea-Bird Electron. Inc.

Seidel, M. P., Degrandpre, M. D. and Dickson, A. G. (2008). A Sensor for *In Situ* Indicator-Based Measurements of Seawater Ph. *Mar. Chem.* 109, 18–28. doi: 10.1016/j.marchem.2007.11.013

Staudinger, C., Strobl, M., Fischer, J. P., Thar, R., Mayr, T., Aigner, D., et al. (2018). A Versatile Optode System for Oxygen, Carbon Dioxide, and pH Measurements in Seawater With Integrated Battery and Logger. *Limnol. Oceanogr. Methods* 16, 459–473. doi: 10.1002/lom3.10260

Stokowski, M., Schneider, B., Rehder, G. and Kuliński, K. (2020). The Characteristics of the CO2 System of the Oder River Estuary (Baltic Sea). *J. Mar. Syst.* 211, 1–11. doi: 10.1016/j.jmarsys.2020.103418

Takeshita, Y., Warren, J. K., Liu, X., Spaulding, R. S., Byrne, R. H., Carter, B. R., et al. (2021). Consistency and Stability of Purified Meta-Cresol Purple for Spectrophotometric pH Measurements in Seawater. *Mar. Chem.* 236, 1–10. doi: 10.1016/j.marchem.2021.104018

Thomas, A., Ramkumar, A. and Shanmugam, A. (2022). CO2 Acidification and its Differential Responses on Aquatic Biota-a Review. *Environ. Adv.* 8, 1–6. doi: 10.1016/j.envadv.2022.100219

Van Dam, B. R. and Wang, H. (2019). Decadal-Scale Acidification Trends in Adjacent North Carolina Estuaries: Competing Role of Anthropogenic CO2 and Riverine Alkalinity Loads. *Front. Mar. Sci.* 6 , 136. doi: 10.3389/fmars.2019.00136

Wallace, R. B., Baumann, H., Grear, J. S., Aller, R. C. and Gobler, C. J. (2014). Coastal Ocean Acidification: The Other Eutrophication Problem. *Estuar. Coast. Shelf. Sci.* 148, 1–13. doi: 10.1016/j.ecss.2014.05.027

Wilson, T. J. B., Cooley, S. R., Tai, T. C., Cheung, W. W. L. and Tyedmers, P. H. (2020). Potential Socioeconomic Impacts From Ocean Acidification and Climate Change Effects on Atlantic Canadian Fisheries. *PloS One* 15, 1–29. doi: 10.1371/journal.pone.0226544

Wright-Fairbanks, E. K., Miles, T. N., Cai, W. J., Chen, B. and Saba, G. K. (2020). Autonomous Observation of Seasonal Carbonate Chemistry Dynamics in the Mid-Atlantic Bight. *J. Geophys. Res. Ocean.* 125, 1–20. doi: 10.1029/2020JC016505

Xu, Y.-Y., Chen, B., Cai, W.-J., Gao, Y., Wanninkhof, R., Salisbury, J., et al. (2017). Short-Term Variability of Aragonite Saturation State in the Central Mid-Atlantic Bight. *J. Geophys. Res. Ocean.* 122, 4274–4290. doi: 10.1002/2017JC012901.Received

Yang, B., Patsavas, M. C., Byrne, R. H. and Ma, J. (2014). Seawater pH Measurements in the Field: A DIY Photometer With 0.01 Unit pH Accuracy. *Mar. Chem.* 160, 75–81. doi: 10.1016/j.marchem.2014.01.005

Yin, T., Papadimitriou, S., Rérolle, V. M. C., Arundell, M., Cardwell, C. L., Walk, J., et al. (2021). A Novel Lab-On-Chip Spectrophotometric pH Sensor for Autonomous *In Situ* Seawater Measurements to 6000 M Depth on Stationary and Moving Observing Platforms. *Environ. Sci. Technol.* 55 (21), 14968–14978. doi: 10.1021/acs.est.1c03517

Zeebe, R. E. and Wolf-Gladrow, D. A. (2001). *CO2 in Seawater: Equilibrium, Kinetics, Isotopes* (Amsterdam: Elsevier). doi: 10.1016/s0924-7963(02)00179-3

Zhao, Y., Liu, J., Uthaipan, K., Song, X., Xu, Y., He, B., et al. (2020). Dynamics of Inorganic Carbon and pH in a Large Subtropical Continental Shelf System: Interaction Between Eutrophication, Hypoxia, and Ocean Acidification. *Limnol. Oceanogr.* 65, 1359–1379. doi: 10.1002/lno.11393

Conflict of Interest: The authors declare that the research was conducted in the absence of any commercial or financial relationships that could be construed as a potential conflict of interest.

Publisher's Note: All claims expressed in this article are solely those of the authors and do not necessarily represent those of their affiliated organizations, or those of the publisher, the editors and the reviewers. Any product that may be evaluated in this article, or claim that may be made by its manufacturer, is not guaranteed or endorsed by the publisher.